

Contrasting size-resolved hygroscopicity of fine particles derived by HTDMA and HR-AMS measurements between summer and winter in Beijing: the impacts of aerosol aging and local emissions

Xinxin Fan^{1*}, Jieyao Liu^{1*}, Fang Zhang^{1#}, Lu Chen¹, Don Collins², Weiqi Xu^{3,4}, Xiaoai Jin¹, Jingye Ren¹, Yuying Wang^{1,5}, Hao Wu¹, Shangze Li¹, Yele Sun^{3,4}, Zhanqing Li⁶

¹State Key Laboratory of Earth Surface Processes and Resource Ecology, College of Global Change and Earth System Science, Beijing Normal University, Beijing 100875, China

²Department of Chemical and Environmental Engineering, University of California Riverside, Riverside, California, USA

³State Key Laboratory of Atmospheric Boundary Layer Physics and Atmospheric Chemistry, Institute of Atmospheric Physics, Chinese Academy of Sciences, Beijing 100029, China

⁴College of Earth Sciences, University of Chinese Academy of Sciences, Beijing 100049, China

⁵School of Atmospheric Physics, Nanjing University of Information Science and Technology, Nanjing 210044, China

⁶Earth System Science Interdisciplinary Center and Department of Atmospheric and Oceanic Science, University of Maryland, College Park, Maryland, USA

*Those authors contribute equally to this work

#Correspondence to: fang.zhang@bnu.edu.cn

Abstract

The effects of aerosols on visibility through scattering and absorption of light and on climate through altering cloud droplet concentration are closely associated with their hygroscopic properties. Here, based on field campaigns in winter and summer in Beijing, we compare the size-resolved hygroscopic parameter (κ_{gf}) of ambient fine particles derived by an HTDMA (Hygroscopic Tandem Differential Mobility Analyzer) to that (denoted as κ_{chem}) of calculated by an HR-ToF-AMS (High-resolution Time-of-Flight Aerosol Mass Spectrometer) measurements using a simple rule with the hypothesis of uniform internal mixing of aerosol particles. We mainly focus on contrasting the disparity of κ_{gf} and κ_{chem} between summer and winter to reveal the impact of atmospheric processes/emission sources on aerosols hygroscopicity and to evaluate the uncertainty in estimating particles hygroscopicity with the hypothesis. We show that, in summer, the κ_{chem} for 110, 150 and 200 nm particles was on average ~10% - 12% lower than κ_{gf} , with the greatest difference between the values observed around noontime when aerosols experience rapid photochemical aging. In winter, no apparent disparity between κ_{chem} and κ_{gf} is observed for those >100 nm particles around noontime, but the κ_{chem}

33 is much higher than κ_{gf} in the late afternoon when ambient aerosols are greatly influenced by local traffic and
34 cooking sources. By comparing with the observation from other two sites (Xingtai, Hebei and Xinzhou, Shanxi)
35 of north China, we verify that atmospheric photochemical aging of aerosols enhances their hygroscopicity and
36 leads to 10%-20% underestimation in κ_{chem} if using the uniform internal mixing assumption. The effect is
37 found more significant for these >100 nm particles observed in remote or clean regions. The lower κ_{chem} is
38 likely resulted from multiple impacts of inappropriate application of density and hygroscopic parameter of
39 organic aerosols in the calculation, as well as influences from chemical interaction between organic and
40 inorganic compounds on the overall hygroscopicity of mixed particles. We also find that, local/regional
41 primary emissions, which result in a large number of externally-mixed BC and POA (Primary Organic Aerosol)
42 in urban Beijing during traffic rush hour time, cause 20-40% overestimation of the hygroscopic parameter.
43 This is largely due to an inappropriate use of density of the BC particles that is closely associated with its
44 morphology or degree of its aging. The results show that the calculation can be improved by applying an
45 effective density of freshly BC (0.25-0.45 g cm⁻³) in the mixing rule assumption. Our study suggest that it is
46 critical to measure the effective density and morphology of ambient BC in particularly in those regions with
47 influences of rapid secondary conversion/aging processes and local sources, so as to accurately parameterize
48 the effect of BC aging on particles hygroscopicity.

49 **1. Introduction**

50 The effects of aerosols on visibility through scattering and absorption of light and on climate through
51 altering cloud droplet concentration are influenced by their hygroscopic growth. Understanding and reducing
52 the uncertainty in prediction of the aerosol hygroscopic parameter (κ) using chemical composition would
53 improve model predictions of aerosol effects on clouds and climate.

54 The hygroscopic properties of both the natural and anthropogenic aerosols, in addition to being affected
55 by its chemical composition (Gunthe et al., 2009), are also affected by the particle mixing state and aging
56 (Schill et al., 2015; Peng et al., 2017a). For example, a recent laboratory study showed that the coexisting
57 hygroscopic species have a strong influence on the phase state of particles, thus affecting chemical interactions
58 between inorganic and organic compounds as well as the overall hygroscopicity of mixed particles (Peng et

59 al., 2016a). The field measurements also demonstrated that the hydrophobic black carbon particles became
60 hygroscopic with atmospheric mixing and aging by organics (i.e. Peng et al., 2017a). In a heavily polluted
61 atmosphere with varied aerosol sources and sinks as well as complex physical and chemical processes, the
62 mixing state and its impact on aerosols hygroscopicity is more complicated. The hygroscopicity of mixed
63 particles and mutual impacts between the components are still poorly understood.

64 Previous studies have shown that the difference between the κ obtained from H-TDMA or CCNc
65 measurements and calculated based on the volume mixing ratio of chemical components. Laboratory results
66 from Cruz and Pandis (2000) indicate that κ_{gf} of internally mixed ammonium sulfate and organic matter is
67 higher than κ_{chem} calculated for assumed uniform internal mixing. But Peng et al (2016a) found that, for sodium
68 chloride and organic aerosols mixed particles, the measured growth factors by H-TDMA were significantly
69 lower than calculations from the mixing rule methods. In some field studies on aged aerosols, the κ was
70 underestimated by the calculation based on uniform internal mixing assumption and thus lead to an
71 underestimation of CCN concentration (Bougiatioti, et al., 2009; Chang, et al., 2007; Kuwata, et al., 2008;
72 Wang, et al., 2010; Ren et al., 2018). However, during primary emission dominated periods, the κ value from
73 calculations based on bulk chemical composition was much higher than that measured by H-TDMA
74 measurements (Zhang et al., 2017). The various results from previous studies suggest distinct effects of
75 aerosols mixing state on their hygroscopicity. Overall, to what extent do the differences depend on the mixing
76 state and the extent of aging of the particles, and how the different atmospheric processes and what kinds of
77 mixing structure of the particles may result in those disparity between measured and calculated hygroscopic
78 parameter have not been clearly clarified by the previous studies. A comprehensive investigation on the causes
79 and magnitude of the effect is with great significance to parameterize the effect of atmospheric
80 processes/emissions of aerosols on particles hygroscopicity in models.

81 In the atmosphere, the κ , which is related to the particle mixing state diversity, varies largely across the
82 size range of ambient fine particles (Rose et al., 2010). However, previous study just compared the κ calculated
83 from bulk chemical composition to that measured by H-TDMA (Zhang et al., 2017). Using size-resolved, not
84 bulk chemical composition measurements in different seasons, is expected to provide more comprehensive
85 understanding and insights of how the aerosols mixing state influence on their hygroscopicity, motivating our

86 analysis that employs size-resolved chemical composition measured by an HR-ToF-AMS in this study. The
87 aim of this paper is to study the hygroscopicity and mixing state characteristics of fine particles in the Beijing
88 urban area, and to reveal the impact of atmospheric processes/sources and mixing/aging on aerosols
89 hygroscopicity and elucidate the uncertainty in calculating the hygroscopic parameter using simple mixing
90 rule estimates based on size-resolved chemical composition. The experiment and theory in the study are
91 introduced in Sect. 2. The comparison between the hygroscopic parameter obtained from the HTDMA and
92 and that calculated using size-resolved chemical composition is discussed in Sect. 3. Conclusions from the
93 study are given in Sect. 4.

94 **2. Experiment and Theory**

95 **2.1. Site and instruments**

96 Two field campaigns are conducted during winter 2016 and summer 2017 of urban Beijing (Fig. 1, BJ:
97 39.97° N, 116.37° E) for measurements of aerosols physical and chemical properties. The BJ site is located at
98 the Institute of Atmospheric Physics (IAP), Chinese Academy of Sciences, which is between the north third
99 and fourth ring roads in northern Beijing. Local traffic and cooking emissions can be important at the site (Sun
100 et al., 2015). The sampling period in cold season was from 16 November to 10 December 2016, during the
101 domestic heating period in Beijing. The sampling period in warm season was from 25 May to 18 June 2017.

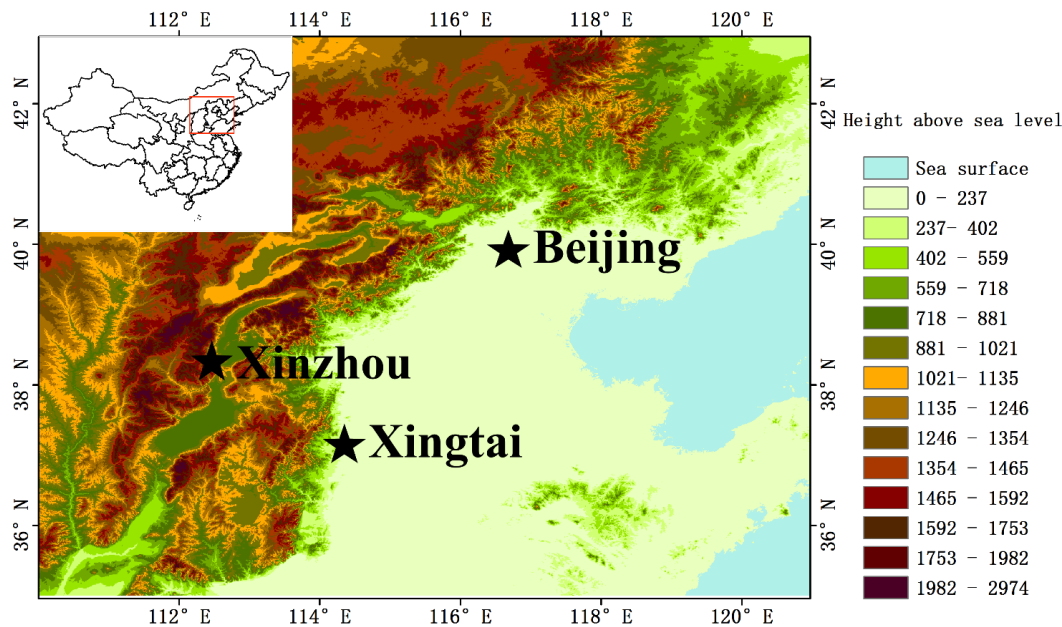


Figure 1. The map location of the sites

Particle number size distribution (PNSD) in the size range from 10 nm to 550 nm was measured with a Scanning Mobility Particle Sizer (SMPS; Wang & Flagan, 1990; Collins et al., 2002), which consists of a long differential mobility analyzer (DMA, model 3081L, TSI Inc) to classify the particle and a condensation particle counter (CPC, model 3772, TSI Inc.) to detect the size classified particles. The sampled particles were dried to relative humidity < 30% before entering the DMA. The measurement time for each size distribution was five minutes.

The HTDMA system used in this study has been described in detail in previous publications (Tan et al., 2013; Wang et al., 2017; Zhang et al., 2017). Here, only a brief description is given. A Nafion dryer dried the sampled particles to relative humidity < 20%, after which the steady state charge distribution was reached in a bipolar neutralizer. The first differential mobility analyzer (DMA₁, model 3081L, TSI Inc.) selected the quasi-monodisperse particles through applying a fixed voltage. The dry diameters selected in this study were 40, 80, 110, 150, and 200 nm. The quasi-monodisperse particles were humidified to a controlled RH (90% in this study) using a Nafion humidifier. A second DMA (DMA₂, same model as the DMA₁) coupled with a water-based condensation particle counter (WCPC, model 3787, TSI Inc.) measured the particle number size

119 distributions of the humidified aerosol. RH calibration with ammonium sulfate was carried out regularly
120 during the study.

121 The hygroscopic growth factor (Gf) is defined as the ratio of the mobility diameter at a given RH to the
122 dry diameter:

$$123 \quad Gf = \frac{D(RH)}{D(dry)}$$

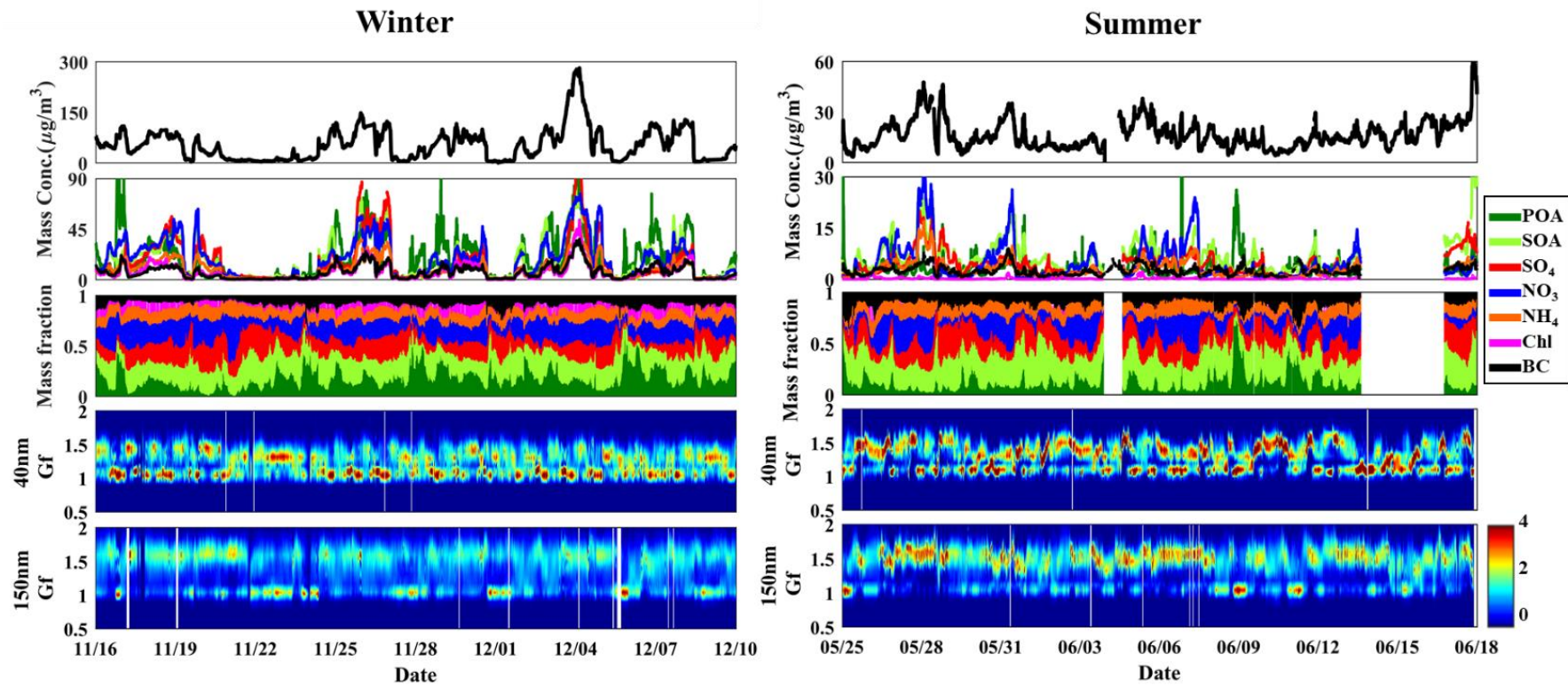
124 The Gf probability density function (PDF) is retrieved based on the TDMA_{inv} algorithm developed by
125 Gysel et al. (2009). Dry scans in which the RH between the two DMAs was not increased were used to define
126 the width of the transfer function.

127 Size-resolved non-refractory submicron aerosol composition was measured with an Aerodyne high-
128 resolution time-of-flight aerosol mass spectrometer (HR-ToF-AMS; Xu et al., 2015). The particle mobility
129 diameter was estimated by dividing the vacuum aerodynamic diameter from the AMS measurements by
130 particle density. Because the uncertainty caused by the fixed density across the size range is negligible (Wang
131 et al. 2016), here, the particle density is assumed to be 1600 kg m⁻³ (Hu et al., 2012). AMS positive matrix
132 factorization (PMF) with the PMF2.exe (v4.2) method was performed to identify various factors of organic
133 aerosols. Xu et al. (2015) have described the operation and calibration of the HR-ToF-AMS in detail. Black
134 carbon (BC) mass concentration was derived from measurements of light absorption with a 7-wavelength
135 aethalometer (AE33, Magee Scientific Corp.; Zhao et al., 2017).

136 **2.2. Data**

137 The time series of the submicron particle mass concentration PM₁, bulk mass concentrations of the main
138 species in PM₁, mass fraction of the chemical composition of PM₁, and probability density function of growth
139 factor (Gf-PDFs) for 40 and 150 nm particles during the campaign are presented in Fig. 2. Quite distinct
140 temporal variability of aerosol chemical and physical properties was observed between winter and summer.
141 The average mass concentration of PM₁ was 55.2 μg/m³ in the winter and 16.5 μg/m³ in the summer during
142 our study periods. In this study, we define the conditions when the mass concentration in winter period was <
143 20 μg m⁻³ and >80 μg m⁻³ as clean and polluted conditions, respectively. Organic aerosol (OA), consisting of

144 secondary organic aerosol (SOA) and primary organic aerosol (POA), was the major fraction during both the
145 winter and summer sampling periods. POA concentration was higher than that of SOA in the winter, which
146 reflects the influence of primary emissions such as coal combustion OA (COOA) in Beijing (Hu et al., 2016;
147 Sun et al., 2016). In contrast, SOA usually dominated in the summer, which is evident that secondary aerosol
148 formation played a key role in the source of PM_{10} . Distinct hydrophobic (with Gf of ~ 1.0) and more
149 hygroscopic (with Gf of ~ 1.5) modes were observed from Gf-PDFs of both small and large particles.
150 Sometimes the more hygroscopic mode particles were more concentrated and at others the hydrophobic
151 particles were. In general though, the more hygroscopic mode dominated for larger particles (i.e. 150 nm),
152 and the less hygroscopic mode did for the smallest particles (e.g. 40 nm). Occasionally, only the hydrophobic
153 mode was evident for 150 nm particles, which occurred when POA dominated the PM_{10} . Only the hygroscopic
154 mode was discernable for 40 nm particles during new particle formation (NPF) events that occurred more
155 frequently in summer than winter (Fig. 3).



156

157

158

Figure 2. Winter (left) and summer (right) time series of mass concentration of PM_{10} , bulk mass concentration of the main species in PM_{10} , mass fraction of the chemical composition of PM_{10} and Gf-PDFs for 40 and 150 nm particles.

2.3. Theory and method

2.3.1 Derivation of the hygroscopic parameter, κ , from the growth factor (Gf)

According to κ -Köhler Theory (Petters and Kreidenweis, 2007), the hygroscopicity parameter κ can be derived using the growth factor measured by an HTDMA.

$$\kappa = (Gf^3 - 1) \left(\frac{\exp\left(\frac{A}{D_d Gf}\right)}{RH} - 1 \right), \quad (1)$$

$$A = \frac{4\sigma_{s/a} M_w}{RT\rho_w}, \quad (2)$$

where Gf is hygroscopic growth factor measured by HTDMA, D_d is the dry diameter of the particles, RH is the relative humidity in the HTDMA (90%, in our study), $\sigma_{s/a}$ is the surface tension of the solution/air (assumed here to be the surface tension of pure water, $\sigma_{s/a} = 0.0728 \text{ N m}^{-2}$), M_w is the molecular weight of water, R is the universal gas constant, T is the absolute temperature, and ρ_w is the density of water.

2.3.2 Derivation of the hygroscopic parameter, κ , from chemical composition data

For an assumed internal mixture, κ can also be calculated by a simple mixing rule on the basis of chemical volume fractions (Petters and Kreidenweis, 2007; Gunthe et al., 2009):

$$\kappa_{chem} = \sum_i \varepsilon_i \kappa_i, \quad (3)$$

where κ_i and ε_i are the hygroscopicity parameter and volume fraction for the individual (dry) component in the mixture, respectively. The AMS provides mass concentrations of organics and of many inorganic ions. The inorganic components mainly consisted of $(\text{NH}_4)_2\text{SO}_4$ and NH_4NO_3 (Zhang et al., 2014). And the values of κ are 0.48 for $(\text{NH}_4)_2\text{SO}_4$ and 0.58 for NH_4NO_3 (Petters and Kreidenweis, 2007). To estimate κ_{Org} , we used the following linear function derived by Mei et al. (2013): $\kappa_{\text{Org}} = 2.10 \times f_{44} - 0.11$. We derived the volume fraction of each species by dividing mass concentration by its density. The density are 1.77 g cm^{-3} for

(NH₄)₂SO₄ and 1.72 g cm⁻³ for NH₄NO₃. The densities of organics are assumed to be 1.2 g cm⁻³ (Turpin et al., 2001). The κ and density of BC are assumed to be 0 and 1.7 g cm⁻³. In the following discussions, κ_{gf} and κ_{chem} denote the values derived from HTDMA measurements and calculated using the ZSR mixing rule, respectively.

In addition, we also compare the results from the field campaigns with those from other two sites, Xingtai (XT: 37.18° N, 114.37° E), and Xinzhou (XZ: 38.24° N, 112.43° E), in North China Plain (Fig. 1). At XZ site, we use the hygroscopic parameter (defined as κ_{CCNc}) from size-resolved CCN measurements (Zhang et al., 2014, 2016) for comparison. More detailed descriptions of the method to retrieve κ_{CCNc} can be found in (Petters and Kreidenweis (2007)). Both of the κ_{gf} and κ_{CCNc} are derived based on κ -Köhler Theory (Petters and Kreidenweis, 2007). But, different from the κ_{gf} measured by the HTDMA system which is operated at RH of 90%, the κ_{CCNc} is derived by measuring aerosols CCN activity under the condition of supersaturations with relative humidity of >100%. Previous studies from filed measurements and laboratory experiments showed that the κ_{CCNc} is generally slight larger or smaller than κ_{gf} , but they are basically comparable and can well represent an overall aerosols hygroscopicity (e.g. Carrico et al., 2008; Wex et al., 2009; Good et al., 2010; Irwin et al., 2010; Cerully et al., 2011; Wu et al., 2013; Zhang et al., 2017).

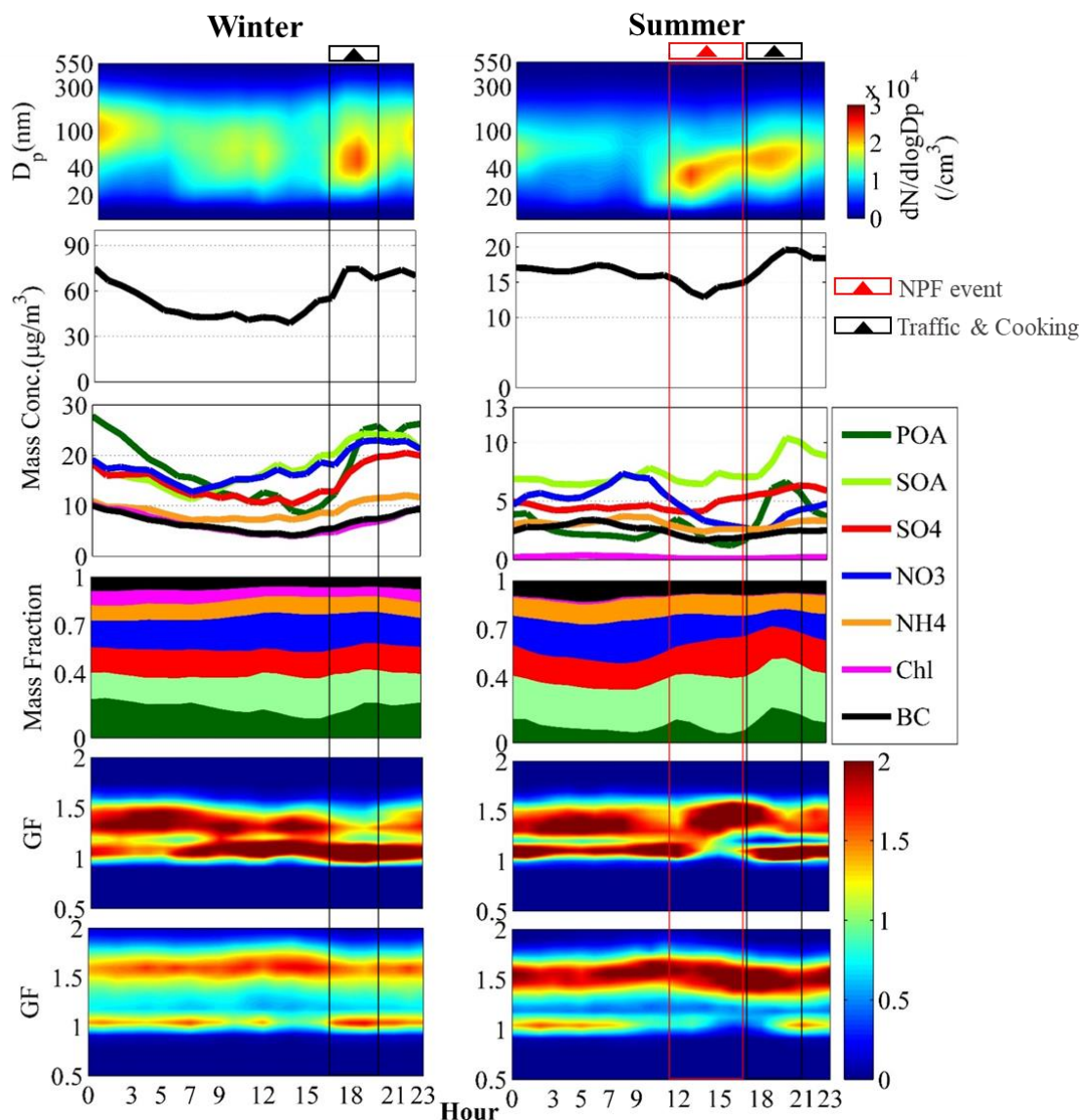
3. Results and discussion

3.1. Diurnal variations of ambient fine particles physiochemical properties and hygroscopic growth factor

The diurnal variations of the PNSD, mass concentration of PM₁, mass concentration and fraction of chemical components in PM₁, and Gf-PDFs for 40 and 150 nm particles during the campaign are shown in Fig. 3. During the summer an obvious peak value in the PNSD is observed around noontime due to NPF events that typically started around 10:00 LT (Local Time). The resulting sharp increase in number concentration of nucleation mode particles was followed by decreased concentration and a rapid growth in diameter of the particles along with increased mass concentration of SOA and sulfate in PM₁, indicating strong photochemical and secondary formation processes during daytime in the summer (Peng et al., 2017b, Marked in red box in

203 Fig. 3). In contrast, NPF was not evident during the winter period, which may in part be due to the much
204 higher ($\sim 3x$) PM_{10} mass concentrations in the winter than in the summer. Note that peak values in number
205 concentration and in mass concentrations of PM_{10} and POA occurred during the early evening (17:00-21:00,
206 LT) indicating the strong impact of local sources from traffic emissions and cooking (Marked in black box in
207 Fig. 3, Peng et al., 2014). In addition, the diurnal cycles of aerosol physical and chemical properties are also
208 influenced by the diurnal changes in the planetary boundary layer (PBL) that leads to accumulation of particles
209 during nighttime when higher values of both number and mass concentration were observed.

210 Owing to the continued local and primary emissions near the study site, the Gf-PDFs for 40 nm particles
211 generally display a bimodal shape with more and less hygroscopic modes (with Gf of ~ 1.5 and ~ 1.1
212 respectively) throughout the day both in winter and summer periods, indicating an external mixing state for
213 the 40 nm particles. Note that, during nighttime and early morning in the winter, the more hygroscopic mode
214 dominated and was shifted to higher Gf than during the daytime. This is thought to be due to
215 heterogeneous/aqueous reactions on pre-existing primary small particles, and/or coagulation/condensation
216 processes that are enhanced at night under lower ambient temperature and higher relative humidity, all of
217 which result in a more hygroscopic and more internally-mixed aerosol (Liu et al., 2011; Massling et al., 2005;
218 Ye et al., 2013; Wu et al., 2016; Wang et al., 2018a). Interestingly, in the summer period, the concentration
219 of the hydrophilic mode increased quickly around noontime and in the early afternoon (12:00-16:00), with a
220 corresponding decrease in the relative concentration of the hydrophobic mode, which likely indicates a
221 transformation of the particles from externally to internally mixing state as a result of the species condensation
222 from the photochemical reaction (Wu et al., 2016; Wang et al., 2017), resulting in an increase in particle
223 hygroscopicity. In addition, it is evident that 40 nm particles after 12:00 were dominated by NPF (Fig. 3).
224 Therefore, the increase of hydrophobic mode particles suggests that a large amount of hydrophilic particles
225 are generated from NPF. For 150 nm particles, the hygroscopic mode in the Gf-PDF is more dominant during
226 daytime in particular during the summer period when the strong solar radiation promotes photochemical aging
227 and growth, thus producing a more internally-mixed aerosol. The dominant hydrophobic mode at around 18:00
228 was observed both in winter and summer and reflects abundant traffic emissions and cooking sources
229 (primarily with POA) during the early evening period.



230

231

232

233

234

Figure 3. Campaign averaged diurnal variations in particle number size distribution; mass concentration of PM_{10} , bulk mass concentration of main species in PM_{10} , mass fraction of chemical composition of PM_{10} ; and Gf-PDFs for 40 and 150 nm particles in winter (left panels) and summer (right panels) measured in urban Beijing..

235

3.2 κ_{gf} dependence on D_p

236

237

238

239

The size dependence of particle hygroscopicity parameters for the winter and summer periods are presented in Fig.4. In the winter, the 40 nm particles were least hygroscopic and the hygroscopicity of larger particles (>80 nm) displayed insignificant dependence on particle size. The size independence for the larger particles is consistent with the observed similarity in mass fractions of inorganic and organic species across

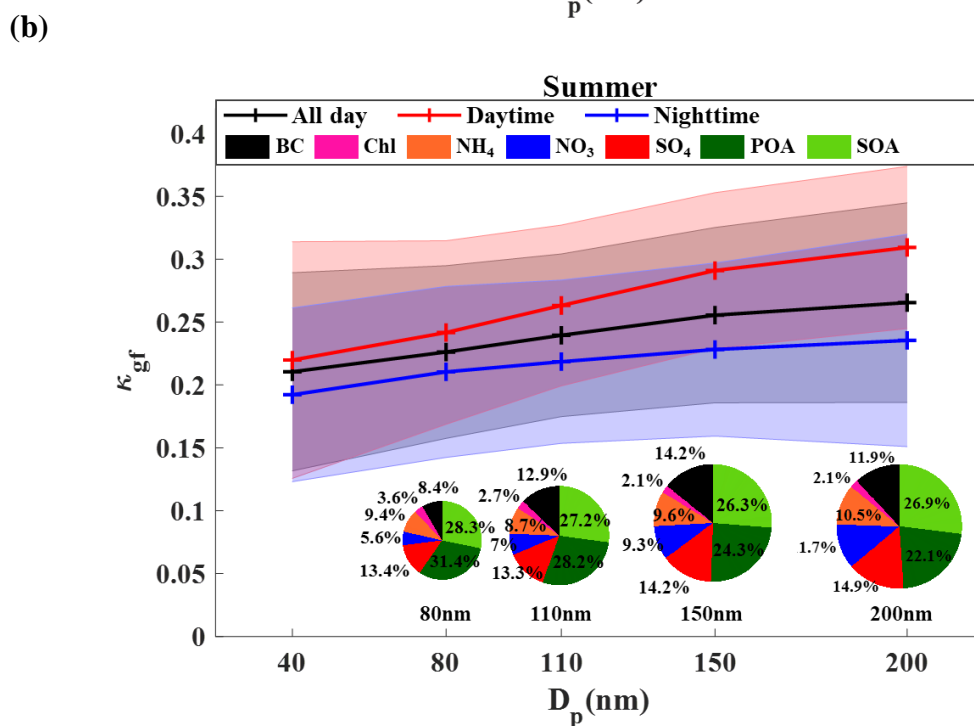
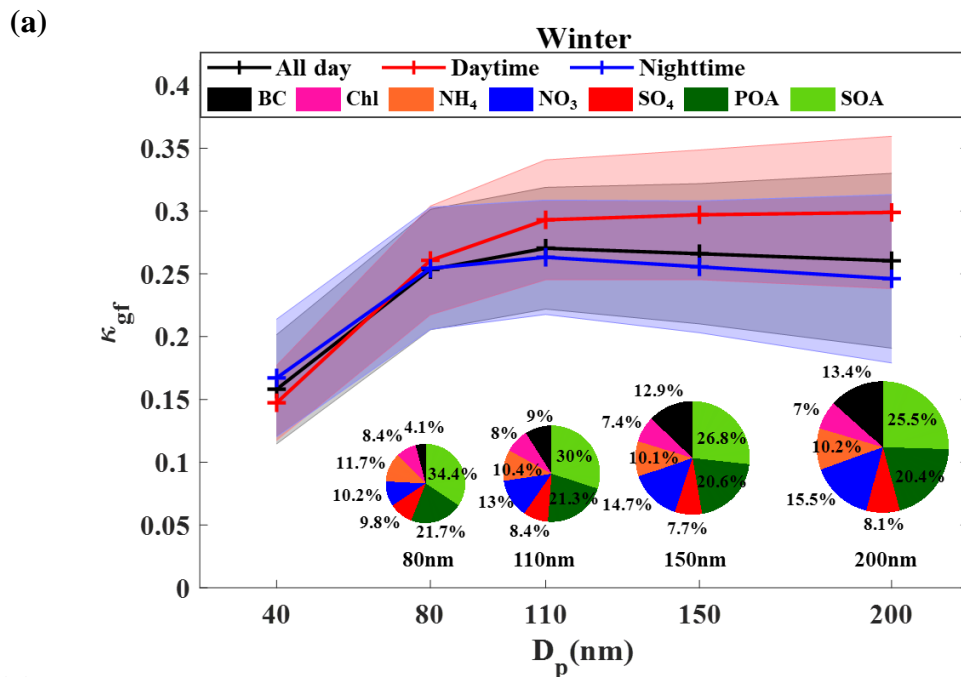


Figure 4. The dependence of κ on D_p at the urban Beijing site during winter (a) and summer (b). The κ values are retrieved from the size-resolved HTDMA measurements. The error bars represent $\pm 1\sigma$. The size-resolved chemical mass fractions at the corresponding D_p is also presented.

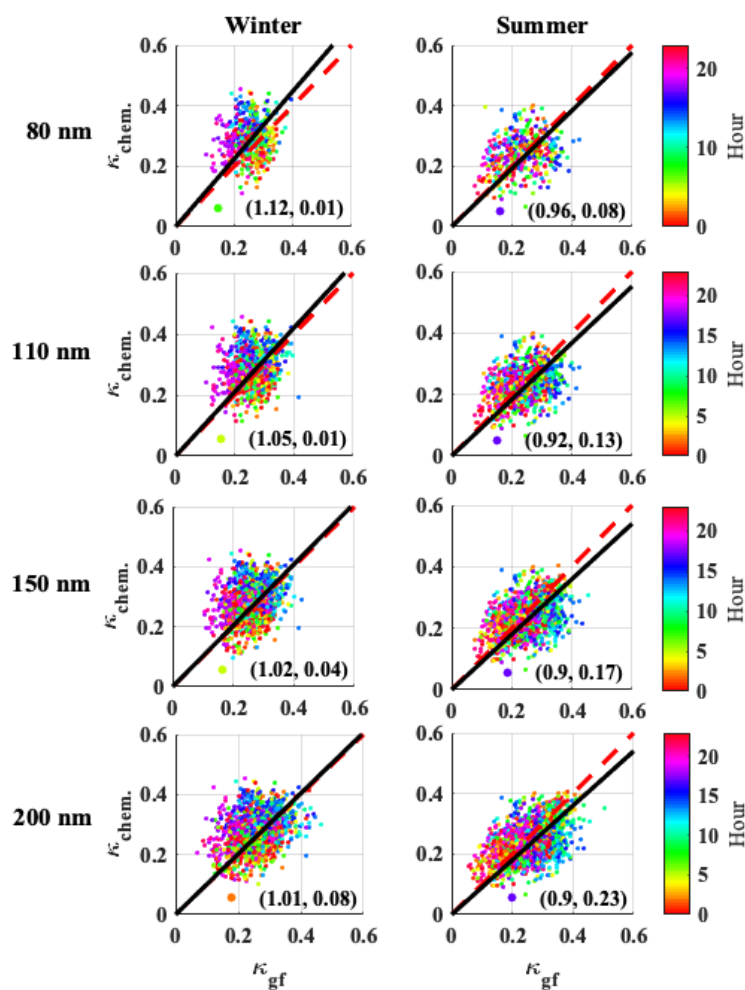
the size range as shown in the pie charts in Figure 4a. A similar dependence of particle hygroscopicity on particle size was also observed in the urban area of Beijing during the wintertime of 2014 (Wang et al., 2018b).

In the summer, hygroscopicity increased with increasing particle size, which is expected based on the size

248 dependent patterns shown in the pie charts, with the mass fraction of POA decreasing with the particles size
249 and the mass fraction of inorganics like sulfate and nitrate increasing with particle size.

250 3.3. Closure of HTDMA and chemical composition derived κ

251 A closure study was conducted between κ_{chem} and κ_{gf} (Fig. 5) to investigate the uncertainty of the two
252 methods, and especially to further illustrate whether particle hygroscopicity can be well predicted by κ_{chem}
253 calculated by assuming internal mixing. Since a size-resolved BC mass concentration measurement was not



254
255 Figure 5. Closure of κ_{chem} calculated from size-resolved chemical composition data and κ_{gf} retrieved from
256 hygroscopic growth factor by HTDMA measurements in winter (left panels) and summer (right panels)
257 period. The dots with different color correspond to observed time of a day during the campaign as shown by
258 the color bar. On each plot, red dotted line is 1:1 line, black solid line is fitting line. The numbers in
259 parentheses are slopes of linear fits and correlation coefficients (R^2).

260

261 available during the campaign, we use the bulk mass fraction of BC particles measured by the AE33 combining
262 with size-resolved BC distribution measured by a single particle soot photometer (SP2) in Beijing (Liu et al.,
263 2018) to estimate κ_{chem} . During the calculation, the BC core diameter measured by SP2 has been converted to
264 the diameter of coated BC particles by multiplying factors of 1.4 and 2.6 under clean (with bulk BC mass
265 concentrations $<2 \mu\text{g m}^{-3}$) and polluted (with bulk BC mass concentrations $>2 \mu\text{g m}^{-3}$) conditions respectively
266 (Liu et al., 2018).

267 Uncertainty in κ is due in part to measurement uncertainty of the HTDMA system and uncertainty
268 resulting from non-ideality effects in the solution droplets, surface tension reduction due to surface active
269 substances, and the presence of slightly soluble substances that dissolve at RH higher than that maintained in
270 the HTDMA (e.g., Wex et al., 2009; Good et al., 2010; Irwin et al., 2010; Cerully et al., 2011; Wu et al., 2013).
271 For example, the HTDMA may overestimate the D_p of dry particles for the external mixed BC particles, as
272 BC-containing particles may shrink when humidified, leading to underestimate the hygroscopic growth factor.
273 However, our previous study demonstrated that, for this region, estimates using HTDMA data are still better
274 representing the aerosols hygroscopicity than those using the simple mixing rule based on chemical volume
275 fractions for an assumed internal mixture (Zhang et al., 2017). Therefore, here we focus on discussing and
276 exploring the uncertainty of κ_{chem} by taking κ_{gf} as the reference.

277 The results show that, although the slopes from linear fitting of κ_{chem} and κ_{gf} are close to 1.0, it is with
278 quite poor correlations (typically with correlation coefficients, R^2 , of <0.3) between κ_{chem} and κ_{gf} of the 80,
279 110, 150, 200 nm particles both in winter and summer. The poor correlations reflect large uncertainty in one
280 or both of the calculated parameters that are likely due to the unreasonable assumption of particle mixing state
281 (e.g. Cruz and Pandis, 2000; Svenningsson et al., 2006; Sjogren et al., 2007; Zardini et al., 2008), which
282 varies with their aging and other physiochemical processes in the atmosphere. Note that underestimation of
283 κ_{chem} for the summer occurred mostly in the afternoon (Marked in blue dots in Fig. 5). This may be associated
284 with photochemical processes at around noontime. More specific investigations of the particle mixing and
285 aging impacts on κ_{chem} will be further addressed in the following sections.

3.4 Aerosols aging and sources effects indicated by diurnal cycles of κ_{chem} and κ_{gf}

The diurnal cycles of particle hygroscopicity in the summer and winter with the use of the size-resolved chemical composition observations and the ratio of κ_{chem} to κ_{gf} are shown in Fig. 6. In summer, at 09:00-15:00, the disparity between κ_{chem} and κ_{gf} is insignificant for smaller particles (80 and 110 nm), both of them show slight decrease from 09:00 or 10:00 to 12:00-13:00 due to the frequent NPF event that usually corresponds to a large fraction of organics (Fig. 3) in urban Beijing. For larger particles (150 and 200 nm), the disparity between κ_{chem} and κ_{gf} around noontime and in the early afternoon is very significant, corresponding to >20% underestimation of particle hygroscopicity by κ_{chem} (with the ratio of κ_{chem} to κ_{gf} of ~ 0.8). Similar patterns were also noted by Zhang et al., (2017) but which is only based on a comparison between κ_{chem} derived from bulk chemical composition and κ_{gf} . Our results based on size-resolved measurements are consistent with that observed by Zhang et al., (2017), and thus again confirming an effect of the rapid photochemical aging of aerosol particles on their hygroscopicity. While, no significant differences between κ_{chem} and κ_{gf} are observed during night time in summer. Note that κ_{chem} is slightly higher than κ_{gf} during early evening traffic rush hour and cooking time, when emissions of primary hydrophobic particles (e.g. BC and POA) are high (Fig. 3), thus resulting in a large percentage of externally-mixed particles). Causes of the overestimation in κ_{chem} during the traffic rush hour and cooking time will be discussed in the following paragraph. The particles experience rapid conversion and mixing in urban Beijing due to high precursor gases (Sun et al., 2015; Wu et al., 2016; Ren et al., 2018), thus the aged particles produced through photochemical processes in the afternoon can mix and interact with the freshly emitted primary particles from traffic and cooking sources (Wu et al., 2008). Therefore, during nighttime (22:00-06:00, LT), the particles are more uniform and internally-mixed, which is reflective of the assumption for calculation of κ_{chem} , a much better consistency between κ_{chem} and κ_{gf} is hence presented.

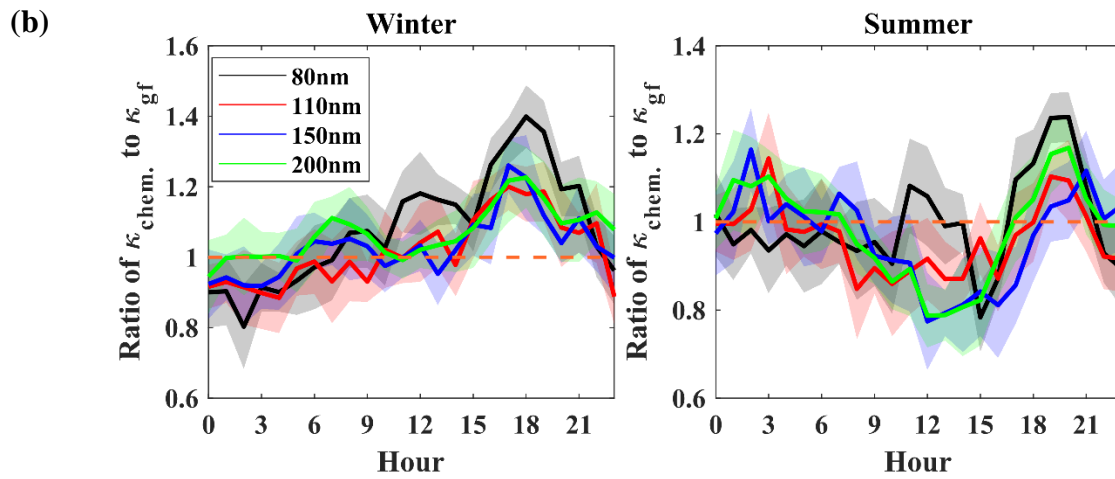
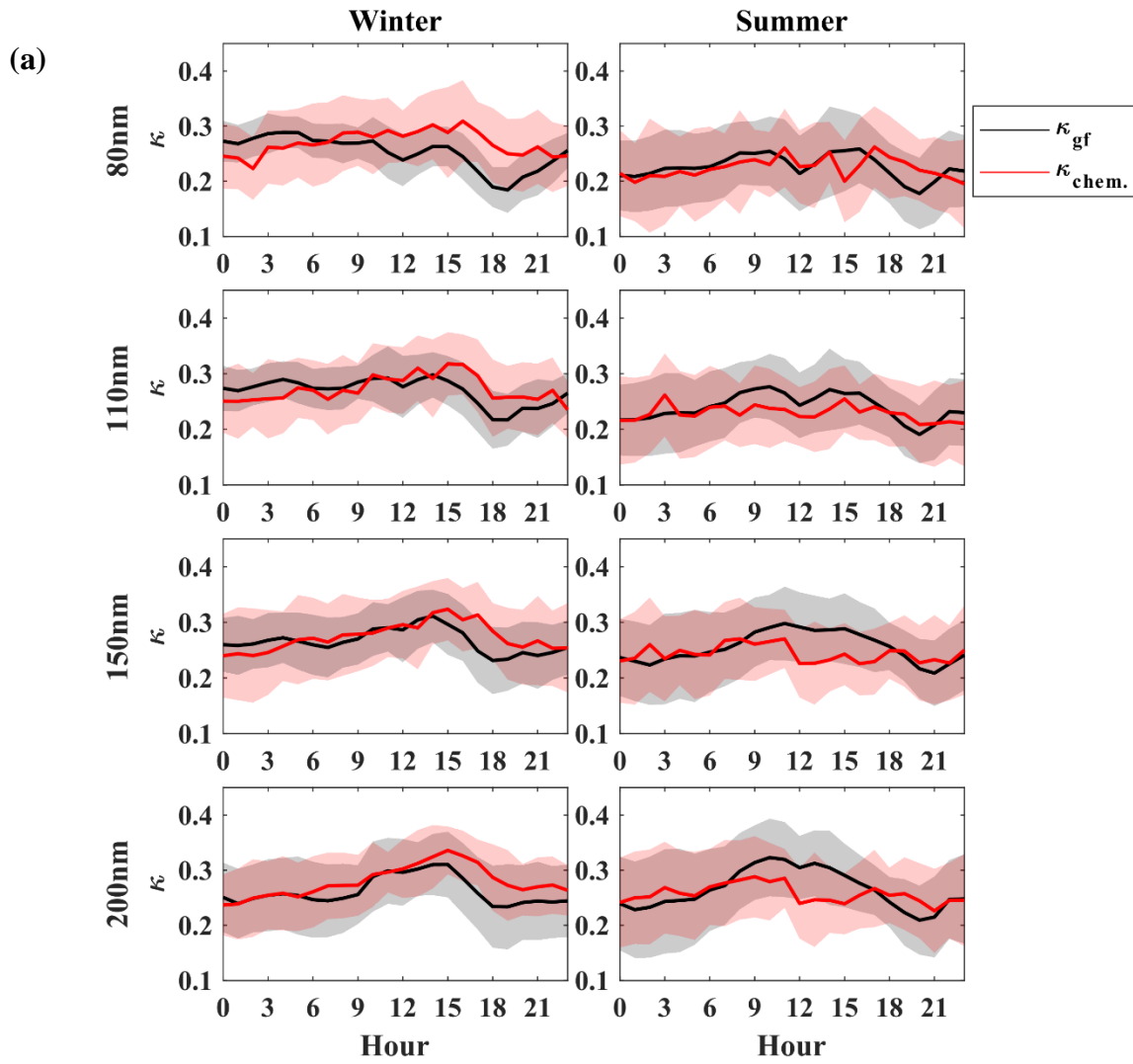
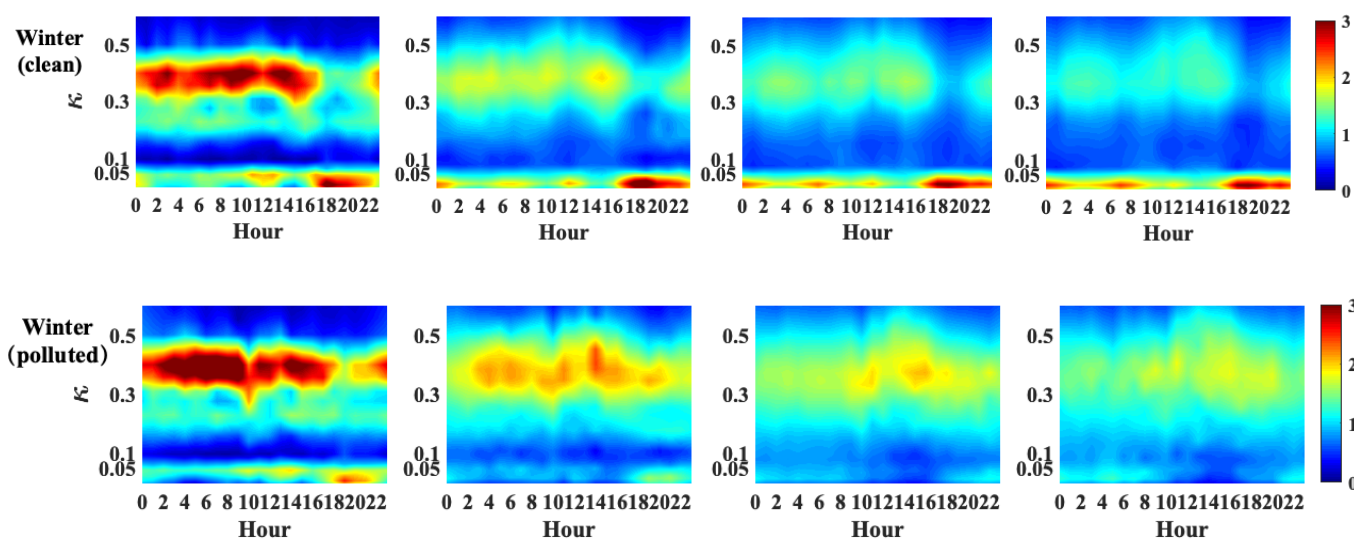


Figure 6. Diurnal variations of (a) κ_{chem} using size-resolved chemical composition data and κ_{gf} in winter and summer period; and (b) ratio of κ_{chem} to κ_{gf} in winter and summer period. The shade regions denote the error bars (1σ).

315 In winter, the disparity between κ_{chem} to κ_{gf} is insignificant at 09:00-15:00 due to the weakening effect of
 316 photochemical aging. From 15:00 to 21:00 LT, due to the strong vehicle and cooking sources around the site,
 317 the particles are dominated by the hydrophobic mode with a large concentration of externally-mixed BC and
 318 POA particles (Fig. 3), the calculated κ_{chem} is much higher than κ_{gf} , with the maximum ratio of κ_{chem} to κ_{gf} of
 319 1.4, and the greatest disparity is observed for small particles. The disparity is further enhanced during clean
 320 periods when the hydrophobic mode is dominant (Fig. 7, Fig. S1). Note that during the nighttime, κ_{chem} is
 321 slight lower than κ_{gf} , with the minimum ratio of κ_{chem} to κ_{gf} of ~ 0.8 for 80 nm particles and ~ 0.9 for 110 and
 322 150 nm particles at 02:00-04:00 LT (Fig. 6b), indicating an underestimation of particle hygroscopicity using
 323 composition data. The disparity at nighttime is further increased during heavily polluted events (Fig. S1),
 324 when the particles are more internally-mixed with only one hygroscopic mode (Fig. 7). We propose the
 325 increased underestimation during polluted conditions is likely due to enhanced condensation of secondary
 326 hygroscopic compounds (e.g. nitrate, sulfate, SOA) on pre-existing aerosols at lower temperature and or
 327 hydrophilic SOA formation under higher relative humidity at nighttime (Wu et al., 2008; Wang et al., 2016;
 328 An et al., 2019). However, such condensation effect during nighttime is less significant (indicated by the
 329 smaller disparity between κ_{chem} and κ_{gf}) than the aging effect caused by aerosols photochemical processes
 330 around noontime (Peng et al., 2016b).



333 Figure 7. Diurnal cycles of κ_{gf} -PDF for 80, 110, 150 and 200 nm particles in clean and polluted events in
 334 winter.

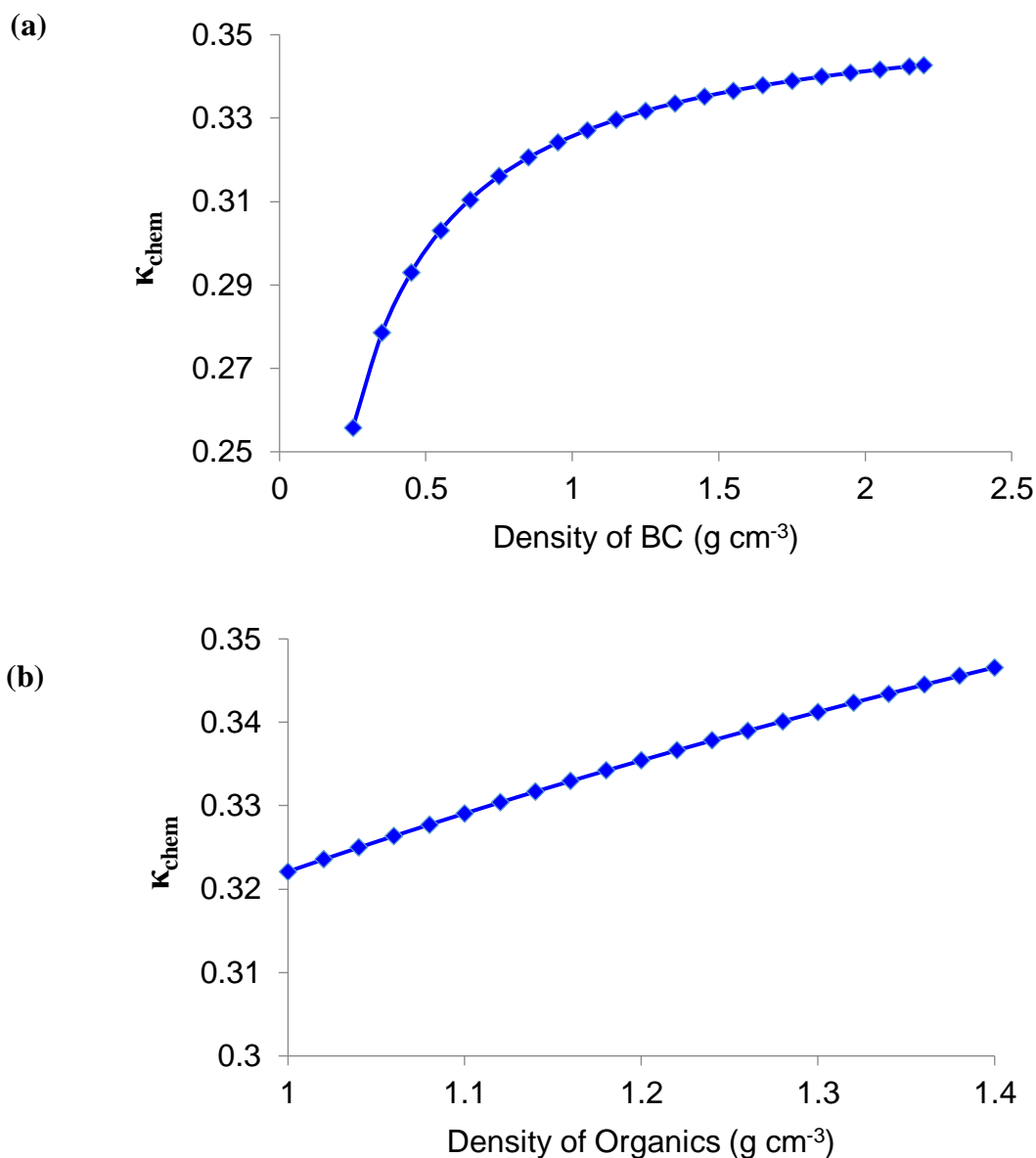
336 We suppose that the higher/lower κ_{chem} should be firstly closely associated with temporal changes in
337 actual effective density of BC with the particles aging/diurnal variations of local emissions. It has been
338 demonstrated that rapid aging of BC can occur over a few hours in the polluted urban area (Peng et al., 2016b).
339 The externally-mixed BC particles are with fractal structure and chain-like aggregates and have been reported
340 with effective density of 0.25-0.45 g cm⁻³(McMurry et al., 2002), while the BC particles in the κ_{chem} calculation
341 is assumed as void free with effective density of 1.7 g cm⁻³. This leads to less BC volume fraction than it
342 actually is and thus the greater κ_{chem} during the traffic rush hour and cooking time when BC particles are
343 mostly freshly emitted with uncompacted structure. In addition, the significant increase in volume fraction of
344 POA during the late afternoon would result in changes of composition of organic aerosols and thereby a
345 density much closer to that of POA than the assumed one (1.2 g cm⁻³) in the calculation should be applied. A
346 sensitivity test has been done to examine the effect of density of BC and organics on calculated κ_{chem} (Fig. 8).
347 The result shows that the κ_{chem} value can be reduced by 16-33% by decreasing the BC effective density from
348 1.7 g cm⁻³ to 0.25-0.45 g cm⁻³. This basically explains the disparity between κ_{chem} and κ_{gf} during the traffic
349 rush hour when a large amount of BC is freshly emitted. The changes in κ_{chem} are within $\pm 4\%$ by varying
350 the organic density from 1.2 (mixture of SOA and POA) to 1.0 (typically for POA) or 1.4 g cm⁻³ (typically for
351 SOA) (Zamora et al., 2019), showing much less impacts of variations of organic density on κ_{chem} . In conclusion,
352 the result demonstrated that the disparity between κ_{chem} and κ_{gf} during late afternoon in winter is largely due
353 to the inappropriate use of the BC particles density that is closely associated with its morphology or degree of
354 its aging. Our study suggest that, to accurately parameterize the effect of BC aging on particles hygroscopicity,
355 it is critical to measure the effective density and morphology of ambient BC, in particularly in those regions
356 with complex influences of rapid secondary conversion/aging processes and local sources.

357 In that way, the lower κ_{chem} value derived around noontime in summer, when BC aerosols may be more
358 compact through strong photochemical aging, is probably due to application of a lower BC density in the
359 calculation. However, the sensitivity test indicates that, to fill the gap between κ_{chem} and κ_{gf} observed at
360 noontime in summer, the effective density of BC should be extremely high due to decreased sensitivity of
361 κ_{chem} to BC density with its aging. In this case, the density of BC has been assumed as 1.7 g cm⁻³, which

362 reflects a very compacted and void free structure of the BC particles. This currently applied value represents
363 an upper limit for the effective density of ambient BC particles according to previous observations near or in
364 Beijing (Zhang et al., 2015), which suggested the aged BC is generally with effective density of 1.2-1.4 g cm⁻³.
365 Using these ambient observed values would lead to further underestimation in κ_{chem} . In addition, the
366 photochemical aging can change the overall effective density of organic aerosols through changing their
367 chemical composition. However, the effective density of the photochemical oxidized organic particles (e.g.
368 SOA) does not change much on the timescale of several hours, and was observed ranging between 1.2 and 1.3
369 g cm⁻³ (Bahreini et al., 2005). It can only explain ~4% at most of the underestimation in κ_{chem} around noontime
370 in summer by applying a density value of 1.4 g cm⁻³ (typically for SOA). Therefore, application of higher
371 densities of BC and organics in the calculation cannot fully explain the disparity between κ_{chem} and κ_{gf} during
372 early afternoon in summer when strong photochemical processes are expected.

373 The uncertainty in calculation of κ_{chem} may be also related to the uncertainty caused by hygroscopic
374 parameter of organics that vary widely over a range of diverse constituents of SOA (Suda et al., 2012). The
375 lower κ_{chem} indicates that the κ of secondary organic aerosols formed through the strong photochemical
376 oxidation processes in summer of urban Beijing are likely underestimated. In this study, the mean κ value of
377 organics derived from the f_{44} parametrized equation is 0.20 ± 0.02 , ranging from 0.17 to 0.23 during 09:00-
378 17:00. While the organic aerosols, especially for particles in accumulated mode, may be more hydrophilic
379 with much larger κ , i.e. >0.2 due to large formation of highly-oxidized OA. One can easily get that increasing
380 the κ of organic aerosols from 0.2 to 0.3 can explain about 11-13% underestimation of κ_{chem} , but representing
381 an upper limit of the impact of hygroscopicity of organic aerosols on the calculation. This is because that the κ
382 value of 0.3 corresponds to the maximum possible for ambient organic aerosols. Additionally, the f_{44}
383 parametrized equation tends to overestimate the κ according to Fröhlich et al. (2015), which should yield a
384 larger κ_{chem} . Finally, the coexisting hygroscopic and hydrophobic species may have a strong influence on the
385 phase state of particles, also likely affecting chemical interactions between inorganic and organic compounds
386 as well as the overall hygroscopicity of mixed particles (Peng et al., 2016a). Overall, The lower κ_{chem} caused
387 by the photochemical aging effect is likely resulted from multiple impacts of inappropriate application of

388 density and hygroscopic parameter of organic aerosols in the calculation, as well as the influences from
389 chemical interaction between organic and inorganic compounds on the overall hygroscopicity of mixed
390 particles. This topic warrants further investigations.



394

395

396

397

398

Figure 8. Sensitivity of κ_{chem} to variations of density of BC (a) and organics (b)

3.5. Observation from other stations

The aging process in the summer period is related to photochemical processing in strong solar radiation conditions. The photochemical reactions produce sulfate and secondary organic aerosol, condensing on the surface of slightly- or non-hygroscopic primary aerosols (such as BC) (Zhang et al., 2008). To confirm such photochemical aging effect on particle hygroscopicity, we further examine the diurnal variations of κ_{chem} and

399 κ_{gf} or κ_{CCNc} (only at XZ site) based on observations in summer at two other sites in north China (Fig. 1). The
400 XT site is located in the suburb of XT city, which is about 400 km south of Beijing, with high levels of
401 industrialization and urbanization. Due to industrial emissions and typically weak ventilating winds,
402 concentrations of $PM_{2.5}$, black carbon and gaseous precursors are usually high at the site (Fu et al., 2014).
403 Xinzhou is located in north of Taiyuan and about 360 km southwest of Beijing, and is surrounded by
404 mountains on three sides. Local emissions from motor vehicles and industrial activities have relatively little
405 influence on the sampled aerosol (Zhang et al., 2016). Because of its location and elevation, the aerosol at the
406 XZ site is usually aged and transported from other areas. The sampling period was from July 22 to August 26,
407 2014 and from May 17 to June 14, 2016 at XZ and XT site respectively.

408 We find that the case at the XT site is very similar to that observed in BJ (Fig. 9a), with a lower κ_{chem} than
409 κ_{gf} around noon time. But, because of much less influences from the local sources at XT compared to that at
410 BJ, such underestimation by κ_{chem} continued until night at XT (Fig. 9b). Interestingly, a noontime lower κ_{chem}
411 was not observed in the diurnal cycles at the XZ site, where κ_{chem} and κ_{CCNc} had similar diurnal patterns (Fig.
412 9c) with a roughly constant ratio of κ_{chem} to κ_{CCNc} of $\sim 0.8-0.9$ (Fig. 9d). This is probably because the XZ site
413 is usually the recipient of aerosols transported from other areas that are already aged and well-mixed, with
414 minimal impact of further aging (Zhang et al., 2017). Also, the rate of oxidation and condensation may be
415 slow in the relatively remote area where the gas precursors and oxidants are not as high as they are closer to
416 sources regions. But at XT, which is located in the heavily polluted area in the north China Plain (Fu et al.,
417 2014), aerosol emissions and processing are more similar to that in urban Beijing. These observations from
418 other sites further confirms the the photochemical aging effect that will largely underestimate the particles
419 hygroscopicity using simple mixing rule based on chemical composition.

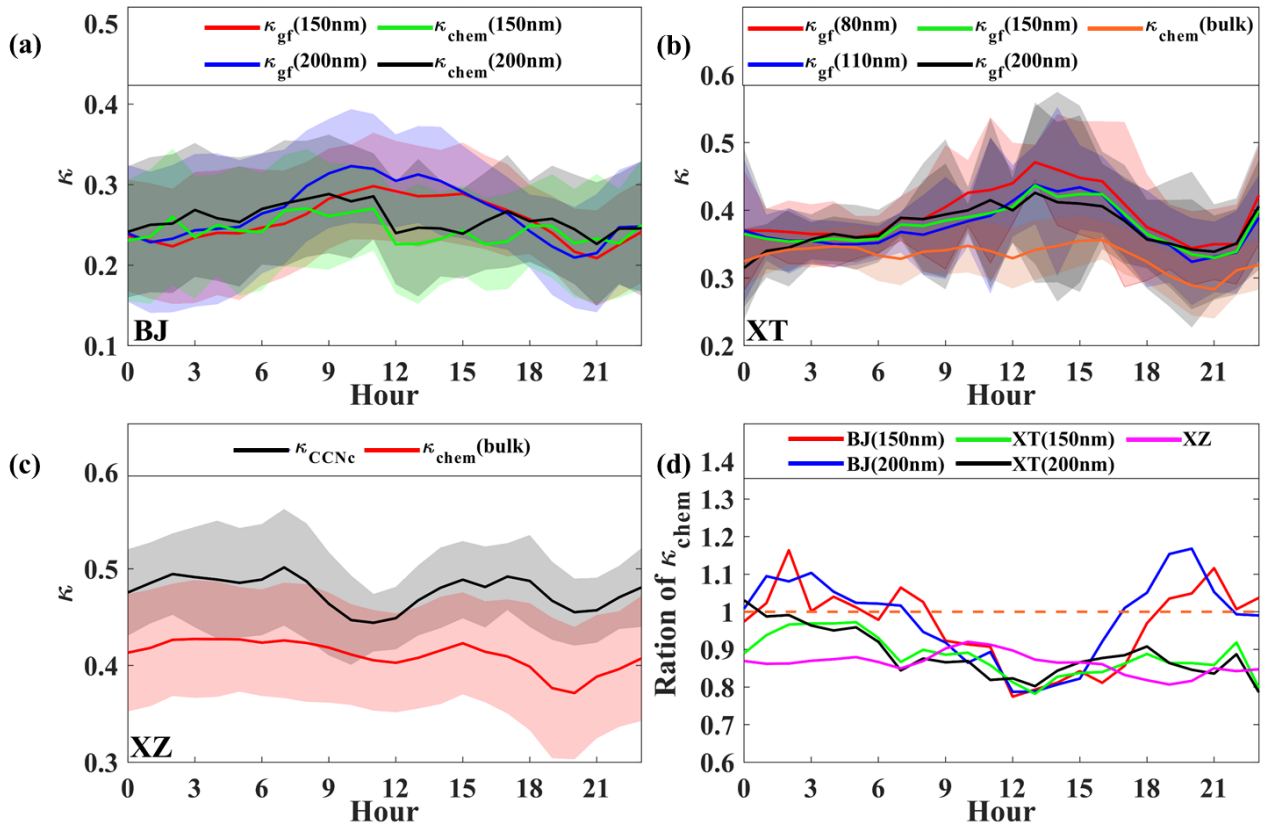


Figure 9. Diurnal variations in (a) κ_{chem} and κ_{gf} for 150 and 200 nm particles at BJ site; (b) κ_{chem} and κ_{gf} for 40, 80, 110, 150 and 200 nm particles at XT site; (c) κ_{chem} and mean κ_{CCNC} for particles at XZ site, and (d) ratio of mean κ_{chem} to κ_{gf} at the three sites.

4. Conclusion

Using measurements of aerosol composition and hygroscopicity made in Beijing (BJ) during a winter period of 2016 and a summer period of 2017, this paper analyzes the daily variation and seasonal differences of size-resolved aerosol hygroscopicity in urban Beijing. We mainly focus on studying the disparity of κ_{gf} and κ_{chem} between summer and winter to reveal the impact of atmospheric processes and mixing state of the particles on its hygroscopicity. The uncertainty in calculating κ by using chemical composition with a uniform internal mixing hypothesis is elucidated from the diurnal variations of the difference between the calculated values: in summer, lower κ_{chem} is obtained around noontime, with a ratio of κ_{chem} to κ_{gf} of about 0.8-0.9 for large particles (i.e. 150 nm and 200 nm), showing an underestimation of particles hygroscopicity by using simple mixing rule based on chemical composition. Combining with the observation from XT and XZ, we attribute the underestimation to the rapid noontime photochemical aging processes in summer, which induces

435 the aging effect that will lead to a lower κ if assuming a uniform mixing of the particles. The lower κ_{chem} is
436 likely resulted from multiple impacts of inappropriate application of density and hygroscopic parameter of
437 organic aerosols in the calculation, as well as the unknown influences from chemical interaction between
438 organic and inorganic compounds on the overall hygroscopicity of mixed particles.

439 In winter, larger κ_{chem} than κ_{gf} for >100 nm particles is derived around noontime and in the early afternoon,
440 with the maximum ratio of κ_{chem} to κ_{gf} of 1.2-1.4 when the particles are dominated by the hydrophobic mode
441 with a large number of externally-mixed POA particles from strong vehicle and cooking sources. We attribute
442 this large disparity between κ_{chem} and κ_{gf} to changes of BC morphology that can be indicated by effective
443 density of BC. The sensitivity test shows that it can well explain the disparity during the traffic rush hour by
444 applying BC effective density of 0.25-0.45 g cm⁻³. However, we suggest that, to accurately parameterize or
445 account for the effect of BC density on particles hygroscopicity, future investigations need to measure the
446 effective density of ambient BC, in particularity in those regions with complex local sources. Our results
447 highlight the impacts of atmospheric processes, sources on aerosol mixing state and hygroscopicity, which
448 should be quantified and considered in models for different atmospheric conditions.

449
450 *Data availability.* All data used in the study are available on

451 <http://www.geodoi.ac.cn/WebCn/doi.aspx?Id=1356> (doi:10.3974/geodb.2019.06.11.V1) or from the
452 corresponding author upon request (fang.zhang@bnu.edu.cn).

453 *Author contributions.* F.Z. and J. L conceived the conceptual development of the manuscript. X. F. directed
454 and performed of the experiments with L.C., X.J., Y. W., and F. Z.. F.Z., J.L., and X.F. conducted the data
455 analysis and wrote the draft of the manuscript, and all authors edited and commented on the various sections
456 of the manuscript. J.L. and X.F. contribute equally to this work.

457 *Competing interests.* The authors declare no competing interests.

458 *Acknowledgements.* This work was funded by National Natural Science Foundation of China (NSFC) research
459 projects (grant nos. 41975174, 41675141), the National Key R&D Program of China (grant no.
460 2017YFC1501702). We thank all participants of the field campaign for their tireless work and cooperation.
461 We also would like to thank the two anonymous reviewers for their insightful and constructive comments.

References

- An, Z., Huang, R. J., Zhang, R., Tie, X., Li, G., Cao, J., Zhou, W., Shi, Z., Han, Y., Gu, Z., and Ji, Y.: Severe haze in Northern China: A synergy of anthropogenic emissions and atmospheric processes, *Proceedings of the National Academy of Sciences*, 116(18), 8657-8666, doi:10.1073/pnas.1900125116, 2019.
- Bahreini, R., Keywood, M. D., Ng, N. L., Varutbangkul, V., and Jimenez, J. L.: Measurements of secondary organic aerosol from oxidation of cycloalkenes, terpenes, and *m*-xylene using an aerodyne aerosol mass spectrometer. *Environ. Sci. Technol.*, 39(15), 5674–5688, 2005.
- Bougiatioti, A., Fountoukis, C., Kalivitis, N., Pandis, S. N., Nenes, A., and Mihalopoulos, N.: Cloud condensation nuclei measurements in the marine boundary layer of the Eastern Mediterranean: CCN closure and droplet growth kinetics, *Atmos. Chem. Phys.*, 9, 7053–7066, doi: 10.5194/acp-9-7053-2009, 2009.
- Carrico, C. M., M. D. Petters, S. M. Kreidenweis, J. L. Collett Jr., G. Engling, and Malm W. C.: Aerosol hygroscopicity and cloud droplet activation of extracts of filters from biomass burning experiments, *J. Geophys. Res.*, 113, D08206, doi:10.1029/2007JD009274. 2008.
- Cerully, K. M., Raatikainen, T., Lance, S., Tkacik, D., Tiitta, P., Petäjä, T., Nenes, A. : Aerosol hygroscopicity and CCN activation kinetics in a boreal forest environment during the 2007 EUCAARI campaign, *Atmos. Chem. Phys.*, 11, 12369–12386, doi: 10.5194/acp-11-12369-2011, 2011.
- Chang, R.-W., Liu, P., Leaitch, W., and Abbatt, J.: Comparison between measured and predicted CCN concentrations at Egbert, Ontario: Focus on the organic aerosol fraction at a semi-rural site, *Atmos. Environ.*, 41, 8172–8182, 2007.
- Collins, D. R., Flagan, R. C., and Seinfeld, J. H.: Improved inversion of scanning DMA data, *Aerosol Sci. Technol.*, 36(1), 1–9, 2002.
- Cruz, C. N. and Pandis, S. N.: Deliquescence and hygroscopic growth of mixed inorganic-organic atmospheric aerosol, *Environ. Sci. Technol.*, 34, 4313–4319, doi: 10.1021/es9907109, 2000.
- DeCarlo, P. F., Kimmel, J. R., Trimborn, A., Northway, M. J., Jayne, J. T., Aiken, A. C., Gonin, M., Fuhrer, K., Horvath, T., Docherty, K., Worsnop, D. R., and Jimenez, J. L.: Field-deployable, high-resolution, time-of-flight aerosol mass spectrometer, *Anal. Chem.*, 78, 8281–8289, doi: 10.1021/ac061249n, 2006.

488 Fors, E. O., Swietlicki, E., Svenningsson, B., Kristensson, A., Frank, G. P., and Sporre, M.: Hygroscopic
489 properties of the ambient aerosol in southern Sweden – a two year study, *Atmos. Chem. Phys.*, 11, 8343–
490 8361, doi: 10.5194/acp-11-8343-2011, 2011.

491 Fröhlich, R., Crenn, V., Setyan, A., Belis, C. A., Canonaco, F., Favez, O., Riffault, V., Slowik, J. G., Aas,
492 W., Aijälä, M., Alastuey, A., Artiñano, B., Bonnaire, N., Bozzetti, C., Bressi, M., Carbone, C., Coz, E.,
493 Croteau, P. L., Cubison, M. J., Esser-Gietl, J. K., Green, D. C., Gros, V., Heikkinen, L., Herrmann, H.,
494 Jayne, J. T., Lunder, C. R., Minguillón, M. C., Mocnik, G., O’Dowd, C. D., Ovadnevaite, J., Petralia, E.,
495 Poulain, L., Priestman, M., Ripoll, A., Sarda-Estève, R., Wiedensohler, A., Baltensperger, U., Sciare, J., and
496 Prévôt, A. S. H.: ACTRIS ACSM intercomparison – Part 2: Intercomparison of ME-2 organic source
497 apportionment results from 15 individual, co-located aerosol mass spectrometers, *Atmos. Meas. Tech.*, 8,
498 2555–2576, doi:10.5194/amt-8-2555-2015, 2015.

499 Fu, G. Q., Xu, W. Y., Yang, R. F., Li, J. B., & Zhao, C. S. : The distribution and trends of fog and haze in the
500 North China Plain over the past 30 years, *Atmos. Chem. Phys.*, 14, 11949-11958, doi: 10.5194/acp-14-
501 11949-2014, 2014.

502 Gasparini, R., R. Li, and D. R. Collins: Integration of size distributions and size-resolved hygroscopicity
503 measured during the Houston Supersite for compositional categorization of the aerosol, *Atmos. Environ.*,
504 38, 3285–3303, doi:10.1016/j.atmosenv.2004.03.019, 2004.

505 Good, N., Topping, D. O., Allan, J. D., Flynn, M., Fuentes, E., Irwin, M., Williams, P. I., Coe, H., and
506 McFiggans, G.: Consistency between parameterisations of aerosol hygroscopicity and CCN activity
507 during the RHaMBLe discovery cruise, *Atmos. Chem. Phys.*, 10, 3189–3203, doi: 10.5194/acp-10-3189-
508 2010, 2010.

509 Gunthe, S. S., King, S. M., Rose, D., Chen, Q., Roldin, P., Farmer, D. K., Jimenez, J. L., Artaxo, P., Andreae,
510 M. O., Martin, S.T., and Pöschl, U.: Cloud condensation nuclei in pristine tropical rainforest air of
511 Amazonia: size-resolved measurements and modeling of atmospheric aerosol composition and CCN
512 activity, *Atmos. Chem. Phys.*, 9, 7551–7575, doi: 10.5194/acp-9-7551-2009, 2009.

513 Gysel, M., Crosier, J., Topping, D. O., Whitehead, J. D., Bower, K.N., Cubison, M. J., Williams, P. I., Flynn,
514 M. J., McFiggans, G.B., and Coe, H.: Closure study between chemical composition and hygroscopic growth

515 of aerosol particles during TORCH2, *Atmos. Chem. Phys.*, 7, 6131–6144, doi: 10.5194/acp-7-6131-2007,
516 2007.

517 Gysel, M., McFiggans, G. B., and Coe, H.: Inversion of tandem differential mobility analyser (TDMA)
518 measurements, *J. Aerosol Sci.*, 40, 134–151, doi: 10.1016/j.jaerosci.2008.07.013, 2009.

519 Hu, W., Hu, M., Hu, W., Jimenez, J. L., Yuan, B., Chen, W., Wang, M., Wu, Y., Chen, C., Wang, Z., Peng,
520 J., Zeng, L., and Shao, M.: Chemical composition, sources, and aging process of submicron aerosols in
521 Beijing: Contrast between summer and winter, *J. Geophys. Res.*, 121, 1955–1977, doi:
522 10.1002/2015JD024020, 2016.

523 Irwin, M., Good, N., Crosier, J., Choularton, T. W., & McFiggans, G.: Reconciliation of measurements of
524 hygroscopic growth and critical supersaturation of aerosol particles in central Germany *Atmos. Chem. Phys.*,
525 10, 11737–11752, doi:10.5194/acp-10-11737-2010, 2010.

526 Jacobson, M.Z. : Strong radiative heating due to the mixing state of black carbon in atmospheric aerosols,
527 *Nature*, 409(6821):695-697, 2001.

528 Kulmala, M., Petaja, T., Monkkonen, P., Koponen, I.K., Dal Maso, M., Aalto, P.P., Lehtinen, K.E.J., and
529 Kerminen, V.M. : On the growth of nucleation mode particles: source rates of condensable vapor in polluted
530 and clean environments, *Atmos. Chem. Phys.*, 5, 409–416, doi: 10.5194/acp-5-409-2005, 2005.

531 Kuwata, M., Kondo, Y., Miyazaki, Y., Komazaki, Y., Kim, J. H., Yum, S. S., Tanimoto, H., and Matsueda,
532 H.: Cloud condensation nuclei activity at Jeju Island, Korea in spring 2005, *Atmos. Chem. Phys.*, 8, 2933–
533 2948, doi:10.5194/acp-8-2933-2008, 2008.

534 Liu, D., Joshi, R., Wang, J., Yu, C., Allan, J. D., Coe, H., Flynn, M. J., Xie, C., Lee, J., Squires, F., Kotthaus,
535 S., Grimmond, S., Ge, X., Sun, Y., and Fu, P.: Contrasting physical properties of black carbon in urban
536 Beijing between winter and summer, *Atmos. Chem. Phys. Discuss.*, doi: 10.5194/acp-2018-1142, in review,
537 2018.

538 Liu, P. F., Zhao, C. S., Göbel, T., Hallbauer, E., Nowak, A., Ran, L., Xu, W. Y., Deng, Z. Z., Ma, N.,
539 Mildenerger, K., Henning, S., Stratmann, F., and Wiedensohler, A.: Hygroscopic properties of aerosol
540 particles at high relative humidity and their diurnal variations in the North China Plain, *Atmos. Chem. Phys.*,
541 3479–3494, doi:10.5194/acp-11-3479-2011, 2011.

- 542 Ma, Y., Brooks, S. D., Vidaurre, G., Khalizov, A. F., Wang, L., and Zhang, R.: Rapid modification of cloud-
543 nucleating ability of aerosols by biogenic emissions, *Geophys. Res. Lett.*, 40, 6293–6297, doi:
544 10.1002/2013GL057895, 2013.
- 545 Massling, A., Stock, M., and Wiedensohler, A.: Diurnal, weekly, and seasonal variation of hygroscopic
546 properties of submicrometer urban aerosol particles, *Atmos. Environ.*, 39(21), 3911–3922, doi:
547 10.1016/j.atmosenv.2005.03.020, 2005.
- 548 McMurry, P. H.; Wang, X.; Park, K.; Ehara, K. The Relationship between Mass and Mobility for Atmospheric
549 Particles. *Aerosol Sci. Technol.*, 36, 227-238, 2002.
- 550 Mei, F., Hayes, P. L., Ortega, A. M., Taylor, J. W., Allan, J. D., Gilman, J. B., Kuster, W. C., de Gouw, J. A.,
551 Jimenez, J. L., and Wang, J.: Droplet activation properties of organic aerosols observed at an urban site
552 during CalNex-LA, *J. Geophys. Res.*, 118, 2903–2917, doi: 10.1002/jgrd.50285, 2013.
- 553 Mikhailov, E. F., Mironov, G. N., Pöhlker, C., Chi, X., Krüger, M. L., Shiraiwa, M., Förster, J. D., Pöschl, U.,
554 Vlasenko, S. S., Ryshkevich, T. I., Weigand, M., Kilcoyne, A. L. D., and Andreae, M. O.: Chemical
555 composition, microstructure, and hygroscopic properties of aerosol particles at the Zotino Tall Tower
556 Observatory (ZOTTO), Siberia, during a summer campaign, *Atmos. Chem. Phys.*, 15, 8847–8869,
557 doi:10.5194/acp-15-8847-2015, 2015.
- 558 Peng, C., Jing, B., Guo, Y. C., Zhang, Y. H., and Ge, M. F.: Hygroscopic behavior of multicomponent aerosols
559 involving nacl and dicarboxylic acids. *J. Phys. Chem. A*, 120(7), 1029-1038, 2016a.
- 560 Peng, J. F., Hu, M., Guo, S., Du, Z., Shang, D., and Zheng, J.: Ageing and hygroscopicity variation of black
561 carbon particles in beijing measured by a quasi-atmospheric aerosol evolution study (quality) chamber.
562 *Atmospheric Chemistry and Physics*, 17(17), 10333-10348, 2017a.
- 563 Peng, J. F., Hu, M., Du, Z. F., Wang, Y. H., Zheng, J., Zhang, W. B., Yang, Y. D., Qin, Y. H., Zheng, R.,
564 Xiao, Y., Wu, Y. S., Lu, S. H., Wu, Z. J., Guo, S., Mao, H. J., and Shuai, S. J.: Gasoline aromatics: a critical
565 determinant of urban secondary organic aerosol formation, *Atmospheric Chemistry and Physics*, 17, 10743-
566 10752, 2017b.
- 567 Peng, J. F., Hu, M., Wang, Z. B., Huang, X. F., Kumar, P., Wu, Z. J., Guo, S., Yue, D. L., Shang, D. J., Zheng,
568 Z., and He, L. Y.: Submicron aerosols at thirteen diversified sites in China: size distribution, new particle

569 formation and corresponding contribution to cloud condensation nuclei production, *Atmospheric Chemistry*
570 *and Physics*, 14, 10249-10265, DOI 10.5194/acp-14-10249-2014, 2014.

571 Peng, J. F., Hu, M., Guo, S., Du, Z. F., Zheng, J., Shang, D. J., Zamora, M. L., Zeng, L. M., Shao, M., Wu, Y.
572 S., Zheng, J., Wang, Y., Glen, C. R., Collins, D. R., Molina, M. J., and Zhang, R. Y.: Markedly enhanced
573 absorption and direct radiative forcing of black carbon under polluted urban environments, *P Natl Acad Sci*
574 *USA*, 113, 4266-4271, 10.1073/pnas.1602310113, 2016b.

575 Petters, M. D. and Kreidenweis, S. M.: A single parameter representation of hygroscopic growth and cloud
576 condensation nucleus activity, *Atmos. Chem. Phys.*, 7, 1961–1971, doi: 10.5194/acp-7-1961-2007, 2007.

577 Ren, J. Y., Zhang, F., Wang, Y. Y., Collins, D., Fan, X. X., Jin, X. A., Xu, W. Q., Sun, Y. L., Cribb, M., and
578 Li, Z. Q.: Using different assumptions of aerosol mixing state and chemical composition to predict CCN
579 concentrations based on field measurements in urban Beijing, *Atmos. Chem. Phys.*, 18, 6907–6921, doi:
580 10.5194/acp-18-6907-2018, 2018.

581 Rose, D., Nowak, A., Achtert, P., Wiedensohler, A., Hu, M., Shao, M., Zhang, Y., Andreae, M. O., and Pöschl,
582 U.: Cloud condensation nuclei in polluted air and biomass burning smoke near the mega-city Guangzhou,
583 China – Part 1: Size-resolved measurements and implications for the modeling of aerosol particle
584 hygroscopicity and CCN activity, *Atmos. Chem. Phys.*, 10, 3365–3383, [https://doi.org/10.5194/acp-10-](https://doi.org/10.5194/acp-10-3365-2010)
585 [3365-2010](https://doi.org/10.5194/acp-10-3365-2010), 2010.

586 Saarnio, K., Frey, A., Niemi, J. V., Timonen, H., Rönkkö, T., Karjalainen, P., Vestenius, M., Teinilä, K.,
587 Pirjola, L., Niemelä, V., Keskinen, J., Häyrinen, A., and Hillamo, R.: Chemical composition and size of
588 particles in emissions of coal-fired power plant with flue gas desulphurization, *J. Aerosol Sci.*, 73, 14–26,
589 2014.

590 Schill, S. R., Collins, D. B., Lee, C., Morris, H. S., Novak, G. A., and Prather, K. A.: The impact of aerosol
591 particle mixing state on the hygroscopicity of sea spray aerosol. *ACS Central Science*, 1(3), 132-141, 2015

592 Sjogren, S., Gysel, M., Weingartner, E., Baltensperger, U., Cubison, M. J., Coe, H., Zardini, A. A., Marcolli,
593 C., Krieger, U. K., and Peter, T.: Hygroscopic growth and water uptake kinetics of two-phase aerosol
594 particles consisting of ammonium sulfate, adipic and humic acid mixtures, *J. Aerosol Sci.*, 38, 157–171,
595 doi: 10.1016/j.jaerosci.2006.11.005, 2007.

596 Suda, S. R., Petters, M. D., Matsunaga, A., Sullivan, R. C., Ziemann, P. J., and Kreidenweis, S. M.:
597 Hygroscopicity frequency distributions of secondary organic aerosols. *J. Geophys. Res.*, 117(D4), D04207,
598 2012

599 Svenningsson, B., Rissler, J., Swietlicki, E., Mircea, M., Bilde, M., Facchini, M. C., Decesari, S., Fuzzi, S.,
600 Zhou, J., Mønster, J., and Rosenørn, T.: Hygroscopic growth and critical supersaturations for mixed
601 aerosol particles of inorganic and organic compounds of atmospheric relevance, *Atmos. Chem. Phys.*, 6,
602 1937–1952, doi: 10.5194/acp-6-1937-2006, 2006.

603 Sun, Y. L., Wang, Z. F., Du, W., Zhang, Q., Wang, Q. Q., Fu, P. Q., Pan, X. L., Li, J., Jayne, J., and Worsnop,
604 D. R.: Long-term real-time measurements of aerosol particle composition in Beijing, China: Seasonal
605 variations, meteorological effects, and source analysis, *Atmos. Chem. Phys.*, 15, 10149–10165, doi:
606 10.5194/acp-15-10149-2015, 2015.

607 Sun, Y., Du, W., Fu, P., Wang, Q., Li, J., Ge, X., Zhang, Q., Zhu, C., Ren, L., Xu, W., Zhao, J., Han, T.,
608 Worsnop, D. R., and Wang, Z.: Primary and secondary aerosols in Beijing in winter: sources, variations
609 and processes, *Atmos. Chem. Phys.*, 16, 8309–8329, doi: 10.5194/acp-16-8309-2016, 2016.

610 Swietlicki, E., Hansson, H. C., HäMeri, K., Svenningsson, B., Massling, A., McFiggans, G., McCurry, P.
611 H., PetÄJÄ, T., Tunved, P., Gysel, M., Topping, D., Weingartner, E., Bal-tensperger, U., Rissler, J.,
612 Wiedensohler, A., and Kulmala, M.: Hygroscopic properties of submicrometer atmospheric aerosol
613 particles measured with H-TDMA instruments in various environments - a review, *Tellus B*, 60, 432–469,
614 doi: 10.1111/j.1600-0889.2008.00350.x, 2008.

615 Tan, H., Xu, H., Wan, Q., Li, F., Deng, X., Chan, P. W., Xia, D., and Yin, Y.: Design and application of an
616 unattended multifunctional H-TDMA system, *J. Atmos. Ocean. Tech.*, 30, 1136–1148, doi:
617 10.1175/JTECH-D-12-00129.1, 2013.

618 Turpin, B. J. and Lim, H. J.: Species contributions to PM_{2.5} mass concentrations: Revisiting common
619 assumptions for estimating organic mass, *Aerosol Sci. Tech.*, 35, 602–610, doi:
620 10.1080/02786820152051454, 2001.

621 Wang, J., Cubison, M. J., Aiken, A. C., Jimenez, J. L., and Collins, D. R.: The importance of aerosol mixing
622 state and size-resolved composition on CCN concentration and the variation of the importance with
623 atmospheric aging of aerosols, *Atmos. Chem. Phys.*, 10, 7267–7283, doi:10.5194/acp-10-7267-2010, 2010.

624 Wang, J., Zhang, Q., Chen, M.-D., Collier, S., Zhou, S., Ge, X., Xu, J., Shi, J., Xie, C., Hu, J., Ge, S., Sun, Y.,
625 and Coe, H.: First chemical characterization of refractory black carbon aerosols and associated coatings
626 over the Tibetan Plateau (4730 m a.s.l), *Environ. Sci. Tech.*, 51, 14072, doi:10.1021/acs.est.7b03973, 2017.

627 Wang, Q., Zhao, J., Du, W., Ana, G., Wang, Z., Sun, L., Wang, Y., Zhang, F., Li, Z., Ye, X., and Sun, Y.:
628 Characterization of submicron aerosols at a suburban site in central China, *Atmos. Environ.*, 131, 115–123,
629 doi:10.1016/j.atmosenv.2016.01.054, 2016.

630 Wang, S. C. and Flagan, R. C.: Scanning Electrical Mobility Spectrometer, *Aerosol Sci. Tech.*, 13, 230–240,
631 1990.

632 Wang, Y., Zhang, F., Li, Z., Tan, H., Xu, H., Ren, J., Zhao, J., Du, W., and Sun, Y.: Enhanced hydrophobicity
633 and volatility of submicron aerosols under severe emission control conditions in Beijing, *Atmos. Chem.*
634 *Phys.*, 17, 5239–5251, doi: 10.5194/acp-17-5239-2017, 2017.

635 Wang Y., Li Z., Zhang Y., Du W., Zhang F., Tan H., Xu H., Fan T., Jin X., Fan X., Dong Z., Wang Q. and
636 Sun Y.: Characterization of aerosol hygroscopicity, mixing state, and CCN activity at a suburban site in the
637 central North China Plain, *Atmos. Chem. Phys.*, 18, 11739-11752, doi: 10.5194/acp-18-11739-2018, 2018a.

638 Wang, Y., Z. Wu, N. Ma, Y. Wu, L. Zeng, C. Zhao, and A. Wiedensohler: Statistical analysis and
639 parameterization of the hygroscopic growth of the sub-micrometer urban background aerosol in Beijing,
640 *Atmos. Environ.*, 175, 184-191, doi: 10.1016/j.atmosenv.2017.12.003, 2018b.

641 Wex, H., Petters, M. D., Carrico, C. M., Hallbauer, E., Massling, A., McMeeking, G. R., Poulain, L., Wu, Z.,
642 Kreidenweis, S. M., and Stratmann, F. :Towards closing the gap between hygroscopic growth and activation
643 for secondary organic aerosol: Part 1—Evidence from measurements, *Atmos. Chem. Phys.*, 9, 3987–3997,
644 doi: 10.5194/acp-9-3987-2009, 2009

645 Wu, Z., Hu, M., Lin, P., Liu, S., Wehner, B., and Wiedensohler, A.: Particle number size distribution in the
646 urban atmosphere of Beijing, China, *Atmos. Environ.*, 42, 7967–7980, doi:
647 10.1016/j.atmosenv.2008.06.022, 2008.

648 Wu, Z. J., Poulain, L., Henning, S., Dieckmann, K., Birmili, W., Merkel, M., van Pinxteren, D., Spindler, G.,
649 Müller, K., Stratmann, F., Herrmann, H., and Wiedensohler, A.: Relating particle hygroscopicity and CCN
650 activity to chemical composition during the HCCT-2010 field campaign, *Atmos. Chem. Phys.*, 13, 7983–
651 7996, doi: 10.5194/acp-13-7983-2013, 2013.

652 Wu, Z. J., Zheng, J., Shang, D. J., Du, Z. F., Wu, Y. S., Zeng, L. M., Wiedensohler, A., and Hu, M.: Particle
653 hygroscopicity and its link to chemical composition in the urban atmosphere of Beijing, China, during
654 summertime, *Atmos. Chem. Phys.*, 16, 1123–1138, doi: 10.5194/acp-16-1123-2016, 2016.

655 Xu, W. Q., Sun, Y. L., Chen, C., Du, W., Han, T. T., Wang, Q. Q., Fu, P. Q., Wang, Z. F., Zhao, X. J., Zhou,
656 L. B., Ji, D. S., Wang, P. C., and Worsnop, D. R.: Aerosol composition, oxidation properties, and sources
657 in Beijing: results from the 2014 Asia-Pacific Economic Cooperation summit study, *Atmos. Chem. Phys.*,
658 15, 13681–13698, doi: 10.5194/acp-15-13681-2015, 2015.

659 Ye, X., Tang, C., Yin, Z., Chen, J., Ma, Z., Kong, L., Yang, X., Gao, W., and Geng, F.: Hygroscopic growth
660 of urban aerosol particles during the 2009 Mirage-Shanghai Campaign, *Atmos. Environ.*, 64, 263–269,
661 doi: 10.1016/j.atmosenv.2012.09.064, 2013.

662 Zamora, M. L., Peng, J., Hu, M., Guo, S., Marrero-Ortiz, W., Shang, D., Zheng, J., Du, Z., Wu, Z., and Zhang,
663 R.: Wintertime aerosol properties in Beijing, *Atmos. Chem. Phys.*, 19, 14329–14338,
664 <https://doi.org/10.5194/acp-19-14329-2019>, 2019.

665 Zardini, A. A., Sjogren, S., Marcolli, C., Krieger, U. K., Gysel, M., Weingartner, E., Baltensperger, U., and
666 Peter, T.: A combined particle trap/HTDMA hygroscopicity study of mixed in-organic/organic aerosol
667 particles, *Atmos. Chem. Phys.*, 8, 5589–5601, doi: 10.5194/acp-8-5589-2008, 2008

668 Zhang, F., Li, Y., Li, Z., Sun, L., Li, R., Zhao, C., Wang, P., Sun, Y., Liu, X., Li, J., Li, P., Ren, G., and Fan,
669 T.: Aerosol hygroscopicity and cloud condensation nuclei activity during the AC3Exp campaign:
670 Implications for cloud condensation nuclei parameterization, *Atmos. Chem. Phys.*, 14, 13423–13437, doi:
671 10.5194/acp-14-13423-2014, 2014.

672 Zhang, F., Li, Z., Li, Y., Sun, Y., Wang, Z., Li, P., Sun, L., Wang, P., Cribb, M., Zhao, C., Fan, T., Yang, X.,
673 and Wang, Q.: Impacts of organic aerosols and its oxidation level on CCN activity from measurement at a
674 suburban site in China, *Atmos. Chem. Phys.*, 16, 5413–5425, doi: 10.5194/acp-16-5413-2016, 2016.

675 Zhang, F., Wang, Y., Peng, J., Ren, J., Zhang, R., Sun, Y., Collin, D., Yang, X., and Li, Z.: Uncertainty in
676 predicting CCN activity of aged and primary aerosols, *J. Geophys. Res.-Atmos.*, 122, 11723–11736, doi:
677 10.1002/2017JD027058, 2017.

678 Zhang, R., Khalizov, A. F., Pagels, J., Zhang, D., Xue, H., and McMurry, P. H.: Variability in morphology,
679 hygroscopicity, and optical properties of soot aerosols during atmospheric processing, *PNAS*, 105(30),
680 10291–10296, doi:10.1073/pnas.0804860105, 2008.

681 Zhang, R., Wang, G., Guo, S. Zamora, M. and Wang. Y.: Formation of urban fine particulate matter. *Chemical*
682 *Reviews*, 115(10), 3803-3855, 2015

683 Zhang, Y., Zhang, Q., Cheng, Y., Su, H., Kecorius, S., Wang, Z., Wu, Z., Hu, M., Zhu, T., Wiedensohler, A.,
684 and He, K.: Measuring the morphology and density of internally mixed black carbon with SP2 and VTDMA:
685 new insight into the absorption enhancement of black carbon in the atmosphere, *Atmos. Meas. Tech.*, 9,
686 1833-1843, 2016.

687 Zhao, J., Du, W., Zhang, Y., Wang, Q., Chen, C., Xu, W., Han, T., Wang, Y., Fu, P., Wang, Z., Li, Z., and
688 Sun, Y.: Insights into aerosol chemistry during the 2015 China Victory Day parade: results from
689 simultaneous measurements at ground level and 260 m in Beijing, *Atmos. Chem. Phys.*, 17, 3215–3232,
690 doi: 10.5194/acp-17-3215-2017, 2017.